JOURNAL OF GEOPHYSICAL RESEARCH, VOL. 111, C11S24, doi:10.1029/2005JC003320, 2006

Dynamical contrasts between pancake and pack ice, investigated with a drifting buoy array

Martin J. Doble[1] and Peter Wadhams[1]

Received 26 September 2005; revised 6 April 2006; accepted 20 June 2006; published 6 October 2006.

[1] The motion of pancake ice was investigated using an array of specialised drifting buoys, deployed into the advancing ice edge of the Weddell Sea in April 2000. The buoys remained in the ice as the pancakes consolidated into a coherent ice sheet, and the study examined the contrasts in dynamics for equivalent periods before and after consolidation. Drift velocities were largely determined by the meridional component, perpendicular to the ice edge. Prior to consolidation, these showed significantly elevated magnitudes at high frequencies (periods shorter than six hours). Scalar velocities were higher than previously reported values, reducing with time and distance from the ice edge. The same trends were not evident from in situ wind data. Derivation of momentum transfer parameters (wind factor, turning angle) was hampered by a lack of reliable wind directions from the outermost buoys, however. Relative motions between buoys were investigated using differential kinematic parameters. These displayed high amplitude, high frequency oscillations in unconsolidated ice, with RMS invariant values up to two orders of magnitude higher than normally reported for Weddell Sea pack ice. The values were found to be strongly dependent on sampling interval, increasing further at intervals less than one hour. In situ winds did not display an equivalent variation, suggesting that wind-forcing was not responsible, and translation under wave action, either internal or surface gravity, was postulated as the forcing.

Citation: Doble, M. J., and P. Wadhams (2006), Dynamical contrasts between pancake and pack ice, investigated with a drifting buoy array, *J. Geophys. Res.*, *111*, C11S24, doi:10.1029/2005JC003320.

1. Introduction

[2] The growth of sea ice in the Antarctic is dominated by the formation of frazil and pancake ice at the outer limits of the ice cover. The pancakes remain unconsolidated while there is sufficient wave energy to prevent them freezing together, but gradually form a consolidated ice sheet as the freezing front moves farther north and leaves them far from the influence of open ocean waves. The unconsolidated zone is typically of the order of 100 km wide [*Doble et al.*, 2003], though it can be up to 270 km wide [*Wadhams et al.*, 1987]. High ocean heat fluxes prevent further significant thermodynamic growth once the pancakes consolidate [*Gordon and Huber*, 1990] and further thickening takes place largely by ridging [*Worby et al.*, 1998]. The formation of pancake ice thus exerts a dominant influence on the thickness achieved by the Antarctic sea ice cover [*Lange and Eicken*, 1991].

[3] The processes by which the ice forms are not well understood, however, since the nature of the ice makes its study very difficult. The small size of the cakes and their constantly changing aggregations preclude the use of satellite feature-tracking methods, e.g. that of Kwok et al. (1998), and make the deployment of conventional in situ instrumentation hazardous. Buoy deployments in the northern Weddell Sea have mostly been unsuccessful due to instrument failure [*Kottmeier et al.*, 1997], with the harsh wave-influenced environment being particularly destructive to floating devices. Few field data have therefore been published on dynamics in frazil and pancake ice. Field experiments in the marginal ice zone (MIZ) have instead tended to focus on instrumenting relatively large floes before recovery a short time afterwards, most notably as part of the MIZEX (Bering Sea, February 1983; Fram Strait, July 1983; Greenland Sea, June–July 1984) and LIMEX (Newfoundland, March 1987 & March 1989) experiments [*Liu et al.*, 1992; *Wadhams and Squire*, 1986; *Wadhams et al.*, 1988]. The only experimental data covering pancake ice and its transition to pack ice come from tank experiments [*Leonard et al.*, 1998; *Onstott et al.*, 1998; *Shen and Ackley*, 1995]. These suffer from something of a scaling problem, since the frazil crystals are 'life-sized' while the range of wave periods and fetch are not.

[4] The small-scale dynamics of the ice cover have thus remained largely unknown, exacerbated by the inability of conventional Argos drifters to resolve the short timescales of pancake motion [*Martinson and Wamser*, 1990]. Such short timescales may have major implications for ice growth and increased ocean-atmosphere heat flux, as well as for ensuring the correct rheology for models of the region. Wind-driven motion of the pancake ice is of particular

[1]Department of Applied Mathematics and Theoretical Physics, University of Cambridge, Cambridge, UK.

0148-0227/06/2005JC003320$09.00

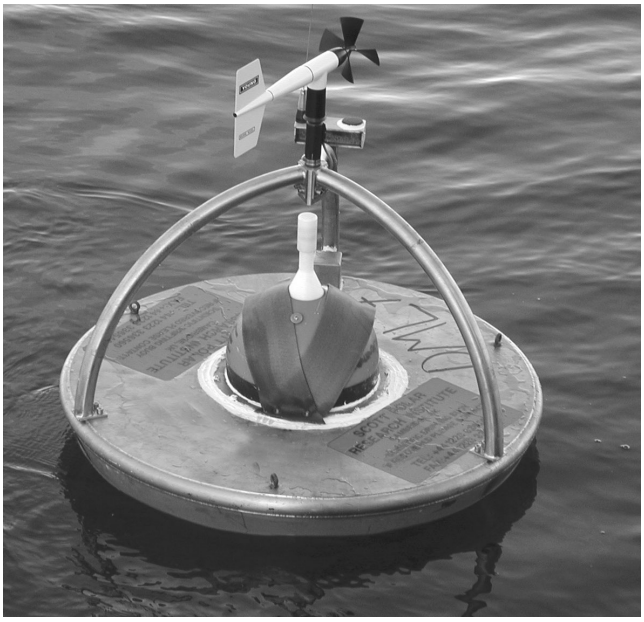

Figure 1. A pancake buoy, shortly after deployment down *Polarstern*'s stern ramp. The steel hull contains the accelerometer and electronics. The wind sensor, Orbcomm and GPS antennae are mounted on the tripod. A MetOcean SVPB is strapped into a well in the hull, as backup to the untried and hastily assembled main system.

interest, since the turning angle and drag coefficient for pancake ice are presently poorly known and models may use values inappropriate to this region.

[5] This paper therefore analyses buoy data from an experiment in the winter marginal ice zone of the central Weddell Sea, designed to study the deformation and dynamics at the smallest scales as the young ice cover evolved from unconsolidated pancakes to the more familiar pack ice. The onset of the consolidation is first discussed and the date of consolidation established. The dynamical contrasts between pancake and pack ice are then examined in time and frequency domains. Momentum transfer and differential kinematic parameters for Antarctic pancake ice are presented for the first time.

2. Description of the Experiment

[6] Six drifting buoys were deployed into the advancing marginal ice zone of the Weddell Sea in April 2000 from the icebreaker *Polarstern*, for the Short Timescale Motion of Pancake Ice (STiMPI) experiment. The buoys reported their GPS position at 20-minute intervals. Wind speed, wind direction and air temperature were measured at 1m above sea level (ASL) every hour [*Meldrum et al.*, 2000a]. The lower-than-normal heights for these meteorological sensors were a necessary result of stability requirements in the heavy icing conditions that the floating buoys were expected to experience. An accelerometer, mounted at the centre of the 1.25 m diameter disc, was used to calculate a vertical displacement wave spectrum every three hours. Data were transmitted over the low-Earth-orbit *Orbcomm* satellite system [*Meldrum et al.*, 2000b].

[7] The buoys were were designed to survive the harsh impact conditions while mimicking the response of the pancakes to wind and waves. They were also designed to freeze into the ice once the pancakes consolidated, with a tapered hull shape allowing the buoys to be squeezed up and out of the ice should significant convergence be encountered. Figure 1 shows one of buoys afloat. The buoys proved to be very robust, with all six units surviving the critical consolidation phase. Details of the deployments and lifetimes are given in Table 1.

[8] The buoys were deployed in a 'five dice' pattern; with one buoy at each corner of a *c*.100 km square and the fifth unit in the centre. The array was positioned near the centre of the Weddell Gyre [*Kottmeier et al.*, 1997], in order to minimize advection and hence maximize residence time in the ice. An additional unit was deployed *c*.300 km further to the west, to verify that the motion of the main array was representative of the ice edge as a whole. This arrangement was found to provide the best compromise between cost and dynamical information in previous MIZ campaigns (e.g. the MIZEX experiments in the Arctic, 1983–9). Buoy tracks for the first two months are shown in Figure 2, which also shows the ice concentration at their deployment, from passive microwave (SSM/I) satellite data. The outer buoys were deployed in new pancakes, while inner buoys were deployed at the limit of the pancake zone, 10–15 km seaward of the northernmost consolidated pack ice. Detailed descriptions of the ice at each location are given in *Doble et al.* [2003].

3. Detection of Consolidation

3.1. Method

[9] The primary aim of the analysis is to contrast the dynamics of pancake ice to those of consolidated pack ice. We therefore need to determine when the ice cover consolidated. The most reliable indicator of this is likely to be the vertical wave spectrum measured by the buoys, since the passage of waves is the physical phenomenon which pre-

Table 1. Buoy Deployment Details[a]

Buoy ID	Argos ID	WMO ID	Position	Deployed	Consol/d	Last Orbcomm	Last Argos
DML4	16187	71583	Inner	19 Apr	20 Apr	15 May	15 May
DML9	19080	71581	Inner	17 Apr	18 Apr	3 Aug	3 Nov
DML5	19075	71511	Centre	18 Apr	29 Apr	13 Oct	24 Oct
DML7	19079	71513	Outer	18 Apr	2 May	30 May	14 Sep
DML8	19076	71512	Outer	17 Apr	3 May	14 Jul	20 Dec
DML6	19081	71582	Long-scale	20 Apr	30 Apr	13 Jul	15 Sep

[a]Columns give the position of the buoy within the ice edge (i.e. outer is farthest north), together with the dates of deployment, consolidation (transition from pancake to pack ice) and last transmission over the two satellite systems. All dates refer to the year 2000.

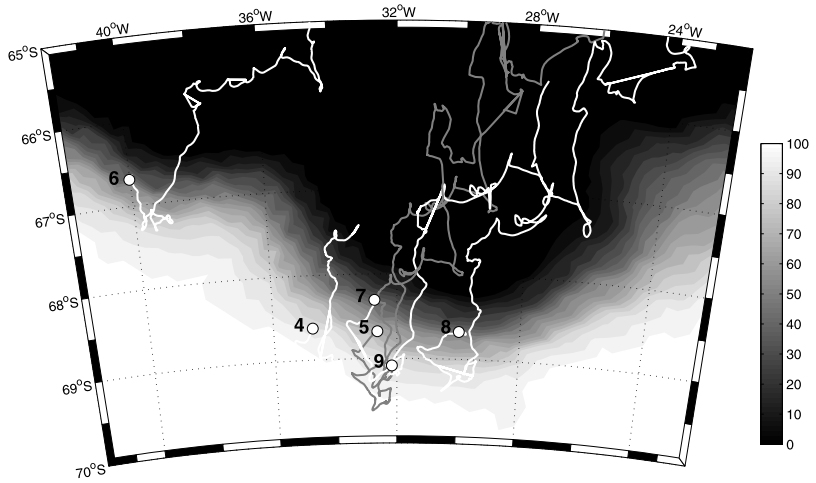

Figure 2. Tracks of all six ice edge buoys. Deployment positions are marked with a yellow circle, together with the ID of each buoy (4 to 9). Background shading shows ice concentration on April 20th (immediately after deployment of the last buoy), as derived from the SSM/I passive microwave satellite sensor.

vents the freezing together of the pancakes and hence maintains the unconsolidated cover [*Wadhams et al.*, 1987].

3.2. Results

[10] Figure 3 shows the significant waveheight and mean period for three representative buoys (outer, middle and inner ice edge) in the main array. Waveheights decreased with distance from the ice edge, with the outer buoys measuring a peak value of around 3 m and inner buoys showing very little vertical motion at any time. Wave motion effectively ceased by May 3rd for all buoys. Mean wave periods showed an evolution from low initial values (7–8 s) at the outer buoys, to a consolidated value of more than 20 s by May 3rd. Inner buoys displayed periods close

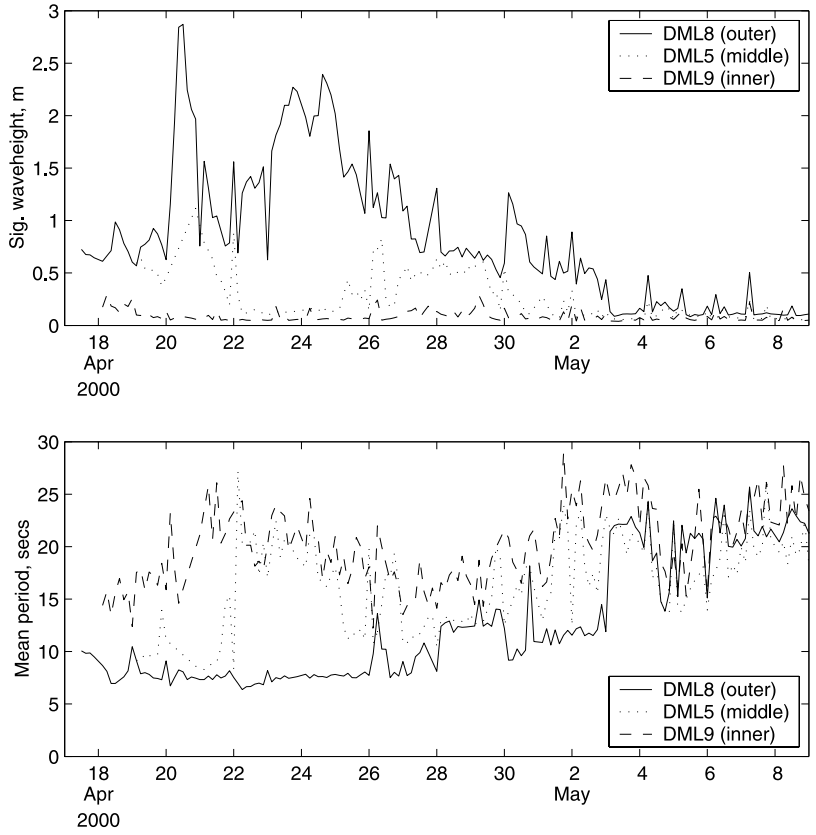

Figure 3. Significant waveheight (top) and mean period (bottom) for outer, middle and inner ice edge buoys.

to 20 s throughout. The exact date of consolidation for each buoy was inferred from examination of the full spectra, and these are shown in Table 1.

[11] The onset of consolidation was also well indicated by the orientation of the buoy with respect to north (buoy heading). In unconsolidated ice, the heading varied rapidly and continuously as the axisymmetric buoys were free to rotate in the water. Once the ice consolidated, the heading remained almost fixed.

3.3. Discussion

[12] The consolidation of the pancakes took place after a rapid advance of the ice edge. The buoys were originally deployed at a slight kink in the otherwise straight edge, but the freezing sea surface advanced northward on either side of the array while remaining essentially stationary at the buoys' longitude, leaving the buoys in a deep ice embayment. This embayment then froze rapidly, with the SSM/I-derived 60% ice concentration contour advancing more than three degrees of latitude between April 30th and May 4th, leaving the buoys far from open water and the influence of wave action. This extensive freezing was driven by both the removal of the wavefield's mechanical constraint and a significant drop in air temperature. Both aspects resulted from a low pressure system passing over the embayment, with its associated winds switching from relatively warm (−2°C), on-ice, northerlies to cold (−17°C), off-ice, southerlies, with reduced fetch and thus reduced ability to raise a significant wavefield. The rapid transition from unconsolidated pancakes to a situation where the buoys are embedded deep within the consolidated pack ice is ideal for comparing dynamical behaviour across a sharp consolidation boundary, and this is done in the following sections.

4. Drift Analysis

[13] Analysis of the buoy drift data is split into three sections; (1) the drift of individual buoys; (2) the transfer functions between buoy drift and wind-forcing; and (3) the relative motion of the buoys in the array. Each is considered first in the time domain then in the frequency domain. Since the drift parameters were expected to vary as the ice cover evolved, calculations were done using a running window, set to 10 days duration, stepping forward at one-day intervals. The window length was chosen to be similar to the duration of the pancake phase of the outer buoys, while providing sufficient samples within the window to allow robust calculations.

[14] Before comparing drift behaviour across the consolidation boundary, it should be noted that the consolidation of the outer buoys on May 2nd and 3rd coincided almost exactly with the ending of the intentional degradation of GPS accuracy available to civilian users. This degradation – termed "Selective Availability" (SA) – was removed at 0430Z on May 2nd 2000. We must therefore be careful to ensure that dynamical differences in the behaviour of pancake and pack ice, derived from these GPS positions, are free from the effects of the varying positional accuracy between SA and non-SA eras.

[15] To this end, we use data from a GPS receiver installed at the German *Neumayer* station (70°39′S, 8°15′W) prior to the experiment. These data showed a gamma distribution with median 18.0 m and variance 143.9 m during the SA era. In the post-SA era, median and variance were 2.8 m and 5.2 m respectively. *Neumayer* data were also used to infer the velocity errors for the buoys, which fitted gamma distributions (P = 0.902 and 0.964, using the Mann-Whitney rank sum test) with median error speeds of 0.89 cm s^{-1} and 0.13 cm s^{-1} and variances of 4.50 cm s^{-1} and 0.03 cm s^{-1} for SA-era and post-SA data respectively. These errors are small in comparison to the c.5 cm s^{-1} accuracy typical for Argos systems, even given typical Argos fix intervals of three hours [*Geiger et al.*, 1998].

[16] When making dynamical comparisons across the boundary, the post-SA (more accurate) data were degraded to SA era accuracy by superimposing positional errors with the SA statistical distribution, applied at a random angle. Positions degraded in this way were statistically similar to the SA era data (P = 0.790) and give considerable confidence that any dynamical differences arose from physical contrasts alone.

4.1. Drift Speed

[17] The buoys had initial scalar drift speeds between 22 and 35 cm s^{-1}. The scalar speed of each buoy was largely determined by its v-component (north-south, approximately perpendicular to the ice edge). The drift speed of all buoys gradually fell during the deployment, reaching a minimum of 18 cm s^{-1} by August. The trend was not reflected in the 10-day average winds, which remained around 4 m s^{-1}. During the initial period, the outer buoys had significantly higher drift speeds (29–35 cm s^{-1} RMS) than the inner buoys (23 cm s^{-1} RMS). The central buoy displayed an intermediate response (28 cm s^{-1} RMS). This disparity was not reflected in the local wind-forcing as measured by the buoys' anemometers. The behaviour was a robust character of the motion, since very similar trends were observed with varying lengths of the running window. Scalar variance, defined as the root-sum-square of the component velocity variances [*Kottmeier et al.*, 1997], was low; at around 2 cm s^{-1}.

[18] Example v-component drift spectra for DML7 (outer MIZ) and DML4 (inner MIZ) are shown in Figure 4, together with those for the scalar in situ wind speed measured at DML7. Spectra are plotted for the pre-consolidation period of DML7 and for an equivalent period (11 days) post-consolidation. Considerable contrast is evident between pre- and post-consolidation spectra for the outer ice edge buoy, with higher power at all frequencies and almost two orders of magnitude increase at high frequencies during the pancake phase. The scalar in situ wind spectra show no such contrast across the consolidation boundary. The inner ice edge buoy displays little change in its spectra over the two periods, however, and the post-May 2nd spectrum is omitted for clarity. Power in both cases is similar to that shown by DML7's post-consolidation spectrum. A significant peak exists in DML7's post-consolidation drift spectrum at around 12 hours. This is an inertial rather than tidal motion, determined using rotary spectra and is also evident in DML4's results.

[19] Scalar drift speeds were higher than other studies found in the region, e.g., 15 cm s^{-1} [*Uotila et al.*, 2000; *Vihma and Launianen*, 1993; *Vihma et al.*, 1996], 17 cm s^{-1} [*Massom*, 1992] and 11 cm s^{-1} [*Geiger et al.*, 2000]. The

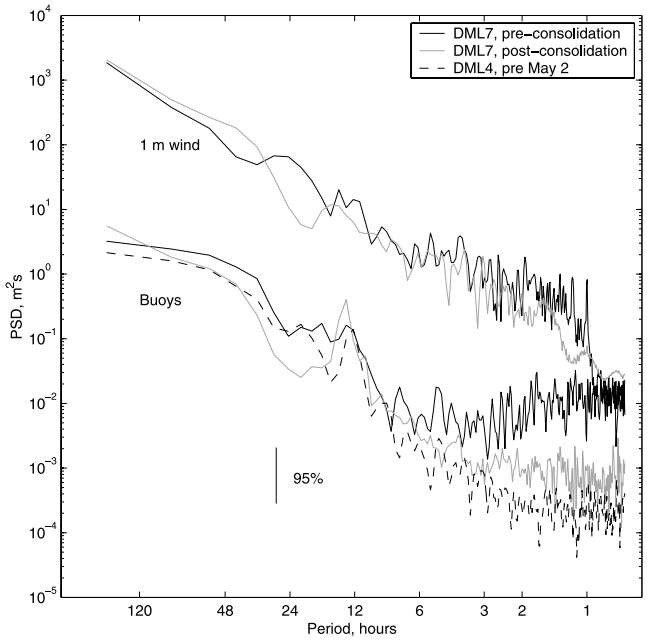

Figure 4. North-south (*v*-component) drift spectra for outer (DML7) and inner (DML4) ice edge buoys. Spectra are presented for similar length periods pre- and post-consolidation for the outer buoy. One spectrum is plotted for the inner buoy, since the post-May 2nd spectrum is very similar to that shown and is therefore omitted for clarity. Also shown are spectra for the scalar in situ wind speed measured at DML7, which show no significant contrast across the consolidation boundary. The 95% confidence interval is marked.

domination of the *v*-component reflected the approximately east-west alignment of the ice edge and the consequent freedom in the north-south direction. Examination of the array shape showed strong variation in north-south separations as passing low pressure systems first compacted the unconsolidated ice with northerly winds, then rarified the ice cover with southerly winds. The pancake ice was unable to transmit the stress necessary to resist deformation, in contrast to consolidated pack ice, and a buoy (or the ice) was thus free to move in response, giving rise to the high speeds observed. As buoys became consolidated, their freedom to respond to wind-forcing was progressively reduced.

[20] The elevated HF portion of the pre-consolidation drift spectrum was not mirrored in the wind record, though the increased sampling interval (1 hour, compared with 20 min for drift) meant that variability at periods shorter than two hours would not be resolved. Elevated drift power densities occurred above approximately six hours in the drift record, however, suggesting that this variability stemmed from other sources. Progressively decreasing drift speeds in the presence of more constant wind-forcing imply variation either in the wind-drift transfer function or in the influence of non-wind-related forcing. This is investigated in the next section.

4.2. Wind Factor and Turning Angle

4.2.1. Method

[21] Momentum transfer from surface winds to buoys or ice can be described by a simple linear ratio, known as the wind factor, α, with a turning angle, δ, between the wind and the forced object (CCW in the Southern hemisphere). Linear ratios have been shown to approximate the non-linear momentum balance well [*Kottmeier et al.*, 1992; *Martinson and Wamser*, 1990; *McPhee*, 1980; *Thorndike and Colony*, 1982], especially for thin Antarctic ice where the Coriolis term is relatively small. Alternative methods, such as the solution of quadratic drag coefficients, involve assumptions about the roughness lengths of air and water interfaces which are unknown [*Thomas*, 1999]. The parameters are important, since they allow the drift of sea ice to be modelled from wind fields provided by numerical weather services.

[22] Wind factor and turning angle were calculated using both the buoy 1 m ASL winds and ECMWF 10 m winds, both interpolated to the 20-minute GPS fix intervals using a cubic spline. Points with a wind speed value of less than 1 m s^{-1} were removed to eliminate sensor freezeup events and light-and-variable conditions. Turning angle was calculated after removing outlying points (those exceeding an absolute turning angle of 120°). In situ wind directions were unfortunately not available from DML6, DML7 and DML8, due to faults in their compasses: though the headings of other buoys varied through the full 360°, primarily during the unconsolidated phase, headings for these outer buoys varied through very limited angles (e.g. 280°–360° for DML7). This is unlikely and points to a fault in these compass units or their calibrations.

[23] ECMWF 10 m were interpolated from the original 1.125° × 1.125° grid to a 0.5° × 0.5° grid. Comparison of in situ and modelled winds showed the ECMWF results to be reasonably accurate once the buoy array became embedded in consolidated pack ice ($0.76 < r_S^2 < 0.89$ – Spearman's rank correlation was used, since the data were non-normal). The correlation was significantly worse near the ice edge ($0.52 < r_S^2 < 0.77$). This is largely ascribed to ice edge thermal and wind stress effects [*Guest et al.*, 1995b], whose mesoscale nature is not resolved by such global models.

[24] Wind factor and turning angle were calculated using both linear regression and a two-parameter matrix solution, described by *Vihma et al.* [1996]. Though generally the most reliable approach, the two parameter method is unable to resolve any parameters for in situ winds from the three invalid-compass buoys, since derivation of the wind factor is no longer divorced from the turning angle. Simple linear regression has its own problems, since it gives rise to non-zero intercepts (drift present in the absence of wind-forcing) which constitute residual currents and integrate the unknown effects of non-wind-based factors, such as wave radiation pressure. The small number of samples available during the unconsolidated phase of many buoys represented a challenge to the regression routine and may have resulted in higher residuals – and consequently lower regression gradients - than would otherwise be the case. We therefore also present results from a third method, which used fixed residuals applied a posteriori to constrain the regression gradient.

4.2.2. Results

[25] Results are shown in Figure 5, for one outer (DML8) and one inner (DML9) ice edge buoy. The wind factor, turning angle and residuals are plotted for the three schemes, for a ten day running window across the first two months of deployment.

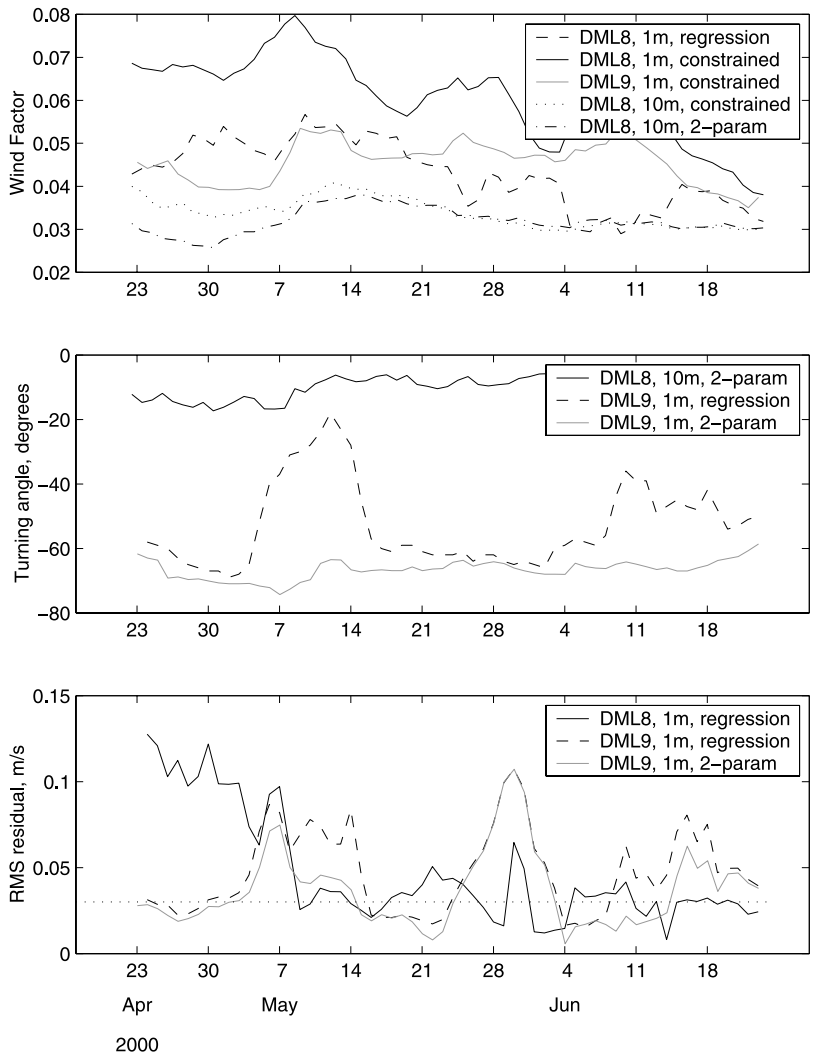

Figure 5. Wind factor and turning angle for outer, middle and inner ice edge buoys.

[26] Simple regression using in situ winds for DML8 showed a downward trend in wind factors, from around 5% to 3% by mid June. Residuals were very high (12 cm s^{-1}) pre-consolidation, reducing gradually to 3 cm s^{-1} in two weeks – a value they remained close to from thereon. This value was therefore chosen for the constrained regression scheme. Other buoys had rather haphazard results with simple regression, reflecting the difficulties of the method with scattered data and a low number of samples. Constrained regression using in situ winds and 3 cm s^{-1} residuals for DML8 showed a clear reduction from around 6.8% in the pancake phase to 3.8% by mid-June. DML9, in contrast showed no clear trend in its constrained regression result with in situ winds, remaining around 4–5% throughout. Constrained regression with 10 m winds and DML8 showed a reduced but similar trend, dropping from 3.5% to 3.0% over the same period, with the inner buoy showing no clear trend and lower values (*c*.2.6%). Two-parameter results were very similar to constrained regression results for 10 m winds. The two-parameter scheme showed little long-term trend with in situ winds for the inner buoy, with values remaining around 4% throughout.

[27] For turning angle, simple and constrained regression gave very similar results for the valid (inner) buoys' in situ winds (*c*. −68°). Two-parameter, 10 m, results were similar for all buoys, staying relatively constant between −10° to −20°. Regression schemes gave similar values to the two-parameter method where the simple regression residuals were low. When these residuals rose, however – due to the low wind speed points being removed and significantly reducing the number of samples available to the algorithms - turning angle was significantly reduced (became less negative). Two-parameter residuals tended to follow a similar form to the regression results, but did not perturb the turning angle, which remained relatively constant throughout.

[28] Correlation coefficients for DML8's 10 m constrained regression rose from a minimum of *c*.0.5 during the pancake phase to a relatively constant 0.85 once consolidation occurred. In situ winds fared rather better during the pancake phase, correlating at $r_S^2 = 0.7$, rising to 0.9 post-consolidation for the constrained regression scheme. Both coefficients for the inner buoy (DML9) remained around 0.85 throughout for in situ winds. For DML9's 10 m winds, both coefficients followed that of DML8 closely.

4.2.3. Discussion

[29] Literature values for pancake ice wind factors are entirely lacking for the Antarctic and sparsely reported for

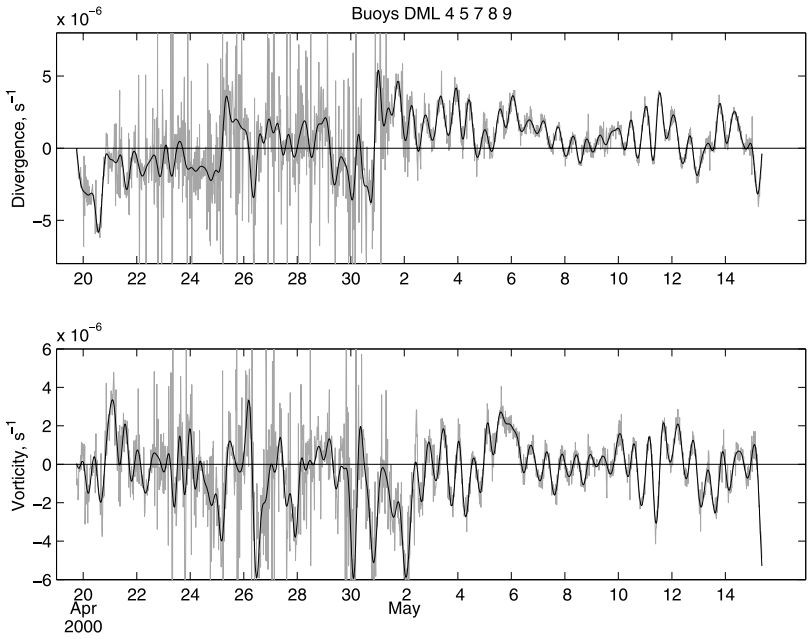

Figure 6. Divergence and vorticity for the full five-buoy array. Drift DKPs are plotted at full resolution (grey) and with a six-hour low-pass filter (solid) and show a dramatic contrast across the consolidation boundary (May 2nd) with the high-amplitude, high-frequency relative motions ceasing almost overnight.

the Northern Hemisphere. For the Odden region of the Greenland Sea, which consists of pancakes with no constraining boundary, *Wilkinson and Wadhams* [2003] reported a 10 m wind factor of 2.7% with a turning angle of 10°. These values were also used by *Pedersen and Coon* [2004] and are broadly consistent with the present study.

[30] Wind factor values for Antarctic pack ice are more common and are widely reported to vary, both seasonally and spatially. Authors variously quote 1.9% (August) to 2.7% October [*Hoeber*, 1991]; 3.4% in the MIZ to 2.4% in pack ice [*Vihma and Launianen*, 1993]; and 1.8% [*Wamser and Martinson*, 1993]. Differences are commonly ascribed to melting, which smoothes the underside of the floes and stabilises the oceanic boundary layer, decreasing momentum exchange and friction [*McPhee*, 1987]. *Vihma and Launianen* [1993] noted that the wind factor depended more on the location of the buoys with respect to the ice edge than seasonal influences.

[31] High residuals and haphazard wind factors suggested that the simple regression scheme was not able to represent the wind-forcing of the buoys in any meaningful manner during the initial period. Constraining the residuals gave more consistent results, but forced all non-wind-related forcing to be taken into the wind factor. The clear trend in DML8's in situ results with this scheme illustrates the decline in influence of these 'other' factors with time.

[32] The two-parameter method is superior, giving consistent results while not suffering undue perturbation of the wind-related factors by variable residuals. The correlation coefficient, particularly the coincident nature of DML8 and DML9's 10 m results, suggest that the performance of the routines during the unconsolidated phase for 10 m winds was more dependent on poor modelled winds than variations in non-wind-related forcing across the array, however. It is unfortunate that the outer MIZ buoys did not provide the in situ wind directions necessary for the two-parameter method to examine results across the consolidation boundary. There are clearly many entangled influences on the momentum transfer operating across the consolidation boundary. Surface current (i.e. water stress) measurements and a full suite of in situ wind data would be required to attribute the various influences on the momentum balance correctly. Variation in wind factor will also occur due to the influence of the larger-scale Weddell Gyre: wind factor will apparently increase if the large-scale wind curl is aligned with the local winds, and vice versa.

4.3. Differential Kinematic Parameters

4.3.1. Method

[33] The relative motions between buoys were next examined for contrasts as the ice cover evolved. These were calculated in terms of the standard differential kinematic parameters (DKPs) [*Crane and Wadhams*, 1996; *Geiger et al.*, 1998; *Kottmeier et al.*, 1997; *Thorndike and Colony*, 1982], which compute the deformation rates of the array using the spatial derivatives of the buoy velocities with respect to the array centroid. We calculate the three invariant terms; divergence, vorticity and maximum shear, by the line integral method as detailed in *Lindsay* [2002], for all five buoys of the main array.

4.3.2. Results

[34] Invariant DKPs were calculated for the five main-array buoys until the failure of the first buoy on May 15th and results for divergence and vorticity are plotted in Figure 6. A dramatic contrast was seen across the consolidation boundary (May 2nd–3rd), with initial high amplitude, high frequency relative motions ceasing almost overnight. The change was almost entirely due to meridional derivatives, particularly dv/dy, which dropped from 4.1 to 1.4 $\times$ 10^{-6} s^{-1} RMS. Actual translation of the array during these high magnitude differential events was small, with mean centroid velocities not exceeding 7 cm s^{-1}.

Table 2. RMS Values for Derivatives and Invariants for Full, Inner (DML 4-5-9) and Outer (5-7-8) Arrays[a]

	4-5-7-8-9 Pre	4-5-7-8-9 Post	4-5-9 Pre	4-5-9 Post	5-7-8 Pre	5-7-8 Post
du/dx, $\times 10^{-6}$ s^{-1}	0.8	0.7	1.4	0.9	1.5	1.3
dv/dx, $\times 10^{-6}$ s^{-1}	0.9	0.8	2.1	1.1	1.6	1.3
du/dy, $\times 10^{-6}$ s^{-1}	2.7	1.2	3.0	1.0	10.0	4.2
dv/dy, $\times 10^{-6}$ s^{-1}	4.1	1.4	5.1	1.2	14.5	3.6
Median spacing, km	82	132	48	80	33	54
Median area, km^2	3390	8733	1186	3212	575	1457
Div, $\times 10^{-6}$ s^{-1}	4.1	1.7	5.1	1.5	14.5	4.0
Vort., $\times 10^{-6}$ s^{-1}	3.0	1.5	4.1	1.4	10.5	4.5
Max Shear, $\times 10^{-6}$ s^{-1}	4.9	2.0	6.4	2.2	17.6	5.6
Div r_S^2 10 m	0.13	−0.23	0.04	−0.10	0.23	−0.21
Vort r_S^2 10 m	0.69	0.72	0.54	0.50	0.31	0.69
Max shear r_S^2 10 m	0.32	0.28	0.22	0.19	0.02	0.30

[a]Values for the drift derivatives and invariants are quoted at full resolution (20 min sampling interval). The correlation coefficients between wind and drift invariants are quoted with the drift values low-pass filtered to match the 'native filter' applied by the wind's sampling interval (i.e. LPF = 12 hours for ECMWF 10 m winds). Winds are rotated by the turning angle, calculated in section 4.2, prior to calculation. The median area of the array over the period of interest (a divisor in calculating the invariants from derivatives) is also tabulated, together with the median spacing between buoys.

Secular divergence was largely negative until May 1st, but became dominantly positive afterwards. The high frequency motion was not a function of the sign of the divergence, however – later prolonged convergent episodes (e.g. June 5th–15th) elicited no such response from the buoys. Vorticity was dominantly negative (clockwise) until May 3rd and then became oscillatory, with a clear semi-diurnal signal that was also evident in the post-consolidation divergence.

[35] Divergence of modelled winds was relatively minor and bore little relation to the buoy results ($r_S^2 = 0.1$ before consolidation, −0.2 afterward). Vorticity was more closely coupled ($r_S^2 = 0.69$ before consolidation, 0.72 afterward), with the envelope of buoy vorticity generally following the wind results. Vorticity was also well-correlated with the sea level pressure measured by the buoys ($r_S^2 = 0.6$). The effects of poor model winds during the unconsolidated phase were difficult to estimate, however, since the lack of in situ wind directions for the outer buoys precluded calculation of 1 m wind DKPs for the array.

[36] To examine variation across the full array, derivatives and invariants were calculated for three-buoy arrays forming the outer (DML 5-7-8) and inner (DML 4-5-9) members, together with their 10 m winds. Results are summarized, along with results for the full array, in Table 2, which shows full-resolution (20 minute sampling interval) results for all derivatives and invariants, together with the scale of each array in terms of the median separation between buoys and the median area. Correlation coefficients compare like with like, applying a low-pass filter to the drift results (12 hour) to match that implied by the sampling interval of the wind data (6 hour). The oscillatory character of the time series, around a near-zero mean, resulted in standard deviation and RMS values being almost identical and hence only RMS values are quoted. The dominant nature of the meridional derivatives is evident, with values for the outer array three times that for the inner or full arrays during the unconsolidated phase. RMS values of the invariants drop by approximately three times across the consolidation boundary in all cases. Correlation coefficients are negligible for divergence in all cases and rather pronounced for vorticity. Vorticity correlation for the outer array more than doubles after consolidation, from 0.31 to 0.69, while values are similar across the boundary for the inner and full arrays. Max shear correlation is low and variable in all cases.

[37] Power spectral densities were calculated on either side of the consolidation boundary for the buoy invariants, and are shown for the divergence of the inner array in Figure 7, together with equivalent spectra for their in situ winds. Drift divergence spectra had similar contrasts to

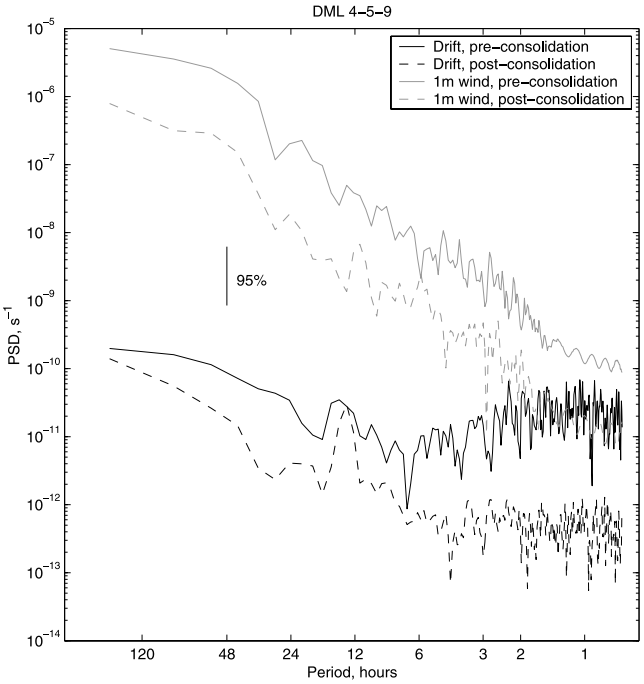

Figure 7. Divergence spectra for the inner, three-buoy, array, for similar-length periods before and after the consolidation. Equivalent spectra for the in situ wind measured by the buoys are also shown. Buoy divergence shows increased power at all frequencies pre-consolidation, but most markedly below 6 hours period. Wind divergence has higher power pre-consolidation, but HF power does not reflect the buoy results. The loss of resolution after two hours period is evident in the wind spectra; a consequence of the one hour sampling interval for these data (compared with 20 min for buoy drift). The 95% confidence interval is marked.

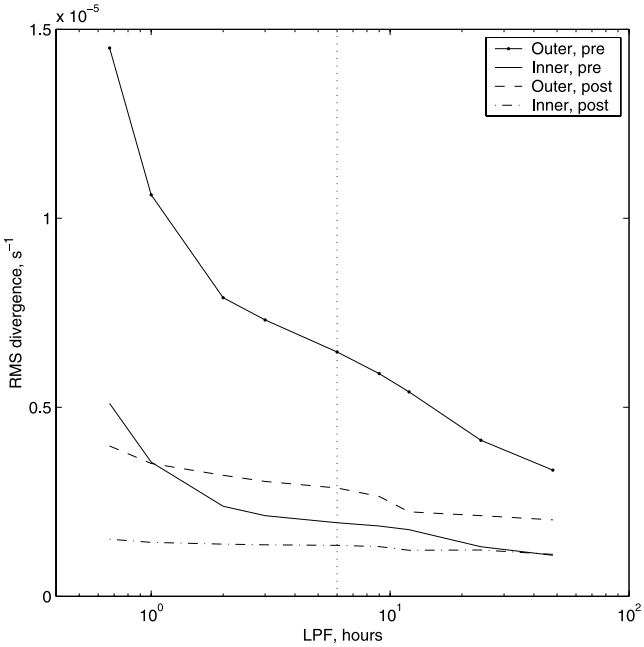

Figure 8. RMS divergence for the outer (DML 5-7-8) and inner (DML 4-5-9) arrays, plotted after the application of various low-pass filters (LPFs). The 'native' low-pass filter, imposed by the sampling interval, is 40 min period. The dotted line indicates the usual limit of Argos-based investigations, at a sampling interval of around three hours (LPF = 6 hours). A distinct break-point in the curve is seen at two hours.

those seen in the drift components themselves: power was higher in the unconsolidated phase, and was especially elevated for periods less than six hours. Wind spectra showed increased power pre-consolidation, presumably due to the more active nature of mesoscale winds near the ice edge, but no evidence of elevated high frequency power. Results for vorticity were similar.

[38] RMS values showed marked variation with the period of the applied LPF, and this prompted examination of the dependence of the magnitude on sampling interval. This was done for all three arrays, calculating values for two periods, corresponding to the unconsolidated phase for the outer buoys and an equivalent period afterward, and results are plotted for divergence in Figure 8. The main feature of the graph is the steep decline in the magnitude of the outer array's pre-consolidation divergence with increasing filter length. A distinct break point occurs at an LPF of two hours, after which the reduction continues at a lesser rate. The pre-consolidation period for the inner array has a similar form, though less exaggerated. A significant reduction in magnitude is seen between pre- and post-consolidation traces for all arrays, but particularly for the outer array, as might be expected. The post-consolidation outer array also shows a step at around 12 hours, following the removal of inertial motions not present in the pre-consolidation record. Results for vorticity were very similar and are not presented.

4.3.3. Discussion

[39] The high amplitude, oscillatory signal in unconsolidated ice is striking and has not been suggested in previous literature. The RMS figures for the unconsolidated DKPs were around two orders of magnitude higher than seen for Weddell Sea pack ice (typically less than 6×10^{-7} s^{-1}) [*Kottmeier et al.*, 1997]. The ice cover is usually considered to display similar magnitudes for du/dx and dv/dy derivatives, resulting in very small divergence signals [*Kottmeier and Sellmann*, 1996]. The meridional preference in the absence of bathymetric influences in the present study clearly arises from the arrays' position at the edge of the ice having a 'free boundary', to the north.

[40] The observed magnitude of the divergence signal (1.5×10^{-5} s^{-1}) implies a relative motion between buoys of around 200 m during the 20 minute fix interval, given the measured area and mutual separations of the array, and has an oscillatory nature (near zero mean). Various forcing mechanisms might exist to produce such motion, and these are discussed in turn below.

4.3.3.1. Mesoscale Wind and Currents

[41] The ice edge is an area of extreme contrasts in both thermal regime and surface roughness. Near the ice edge, in a strip of a width of a few baroclinic Rossby radii, the wind stress profiles are affected by several factors such as the roughness and compactness of the ice as well as by the stability of the atmospheric boundary layer [*Guest and Davidson*, 1991]. Such spatial variations of the wind stress give rise to divergences or convergences of the Ekman transport near the edge and thus generate up- or downwelling, and oceanic jets. Additionally, the surface temperature gradient across the MIZ generates a secondary circulation, or "ice breeze", causing atmospheric boundary layer convergence and deformation. This convergence effect is increased by the contrast in wind turning angles between water (relatively smooth) and MIZ ice (rough). Both effects favour the establishment of sharp, quasi-stationary temperature fronts, wind speed jets and strong vertical velocities near the ice edge. The effects are very sensitive to the balance between the ice breeze and geostrophic wind speeds and the exact angle of both relative to the ice edge [*Guest et al.*, 1995a], particularly in the case of winds parallel to the ice edge.

[42] All of these factors suggest that the outer buoys will experience a significantly altered wind and/or current forcing to the inner buoys in the array. The in situ wind speed records, though showing differences between buoys, do not support a step change in high frequency wind-forcing, however. It is also not clear how the forcing could be dominantly oscillatory. We cannot evaluate the role of water stress, since no current information was acquired, though it appears unlikely that ice edge currents would vary at the very high frequency observed, or, again, be oscillatory.

4.3.3.2. Surface Waves

[43] The role of surface waves in driving the pancakes is difficult to estimate. The usual mechanism, wave radiation pressure [*Longuet-Higgins and Stewart*, 1964], is applicable to objects whose dimensions are comparable with the wavelength of the driving waves. This is clearly not the case for pancakes, whose sub-metre diameters are around two orders of magnitude less than the wavelength of the shortest period waves impinging on them (*c*.150 m for a 10 s period wave). Accordingly, the energy reflection coefficient [*Wadhams*, 1973] becomes vanishingly small and very little force is imparted to the pancake.

[44] An equivalent theory for the wave-induced motion of smaller elements was introduced by *Ruhmer et al.* [1979], who accounted for the ice elements sliding down a wave slope. The approach was developed by *Hopkins and Shen* [2001], who added collisions to the model and simulated pancake drift numerically. Though an exact formulation for the real drift speed is hard to determine, and appears to be rather sensitive to wave amplitude, it is stated that the ice drift velocity approaches the water surface velocity at low amplitudes [*Hopkins and Shen*, 2001]. Taking a typical wave amplitude in the pancake zone as 1 m, with a 10s period, their formulation gives an ice drift of around 18 cms^{-1}, or 216 m between GPS fixes. This motion is similar to the observed magnitude, though such a mechanism does not easily account for the oscillatory signal seen, since the waves drive the pancakes only in the down-wave direction.

4.3.3.3. Internal Waves

[45] The observed motion might arise from coupling between internal waves and surface velocity. This was considered by *Muench et al.* [1983] in the formation of ice edge bands, though velocities in their shallow water case were insufficient to explain the observed motion. In the present case, CTD casts at each deployment station measured a density difference of 0.25 kg m^{-3} across the thermocline, which existed between depths of 60 and 110 m. This gives a Brunt-Väisälä frequency of 7×10^{-3} Hz, or a buoyancy period of around 15 min. The maximum surface velocity that an internal wave of this frequency will produce is around $3 \times 10^{-2}A$, where A is the amplitude of the vertical displacement at the interface. This might be of order 10 m, giving a maximum horizontal velocity at the surface of 30 cm s^{-1}. The displacement integrated over one half period of the internal wave is therefore around 70 m, and internal waves thus appear to be a viable candidate for the observed motion.

[46] Translation under wave action, whether surface or internal, may thus account for the elevated high frequency power observed. Clearly, the consolidation process removes such forcing and can account for the contrast between results for the two ice types.

[47] Anomalous motion has been observed previously, during the MIZEX West experiments in the Bering Sea. Though never published, radar transponders mounted on small floes were observed to circulate within ice edge bands. A complex interaction of short period waves within the band was postulated, though never developed.

[48] The increasing magnitude of the invariants with decreasing sampling interval prompts the question of how much greater the magnitude would be with an even shorter fix interval, and, concomitantly, how small an interval would be feasible before positional errors became significant. Errors are difficult to estimate realistically, but if we assume a square array with buoys at each vertex, at mutual distance d, then an upper bound for the deformation error is [*Lindsay*, 2002]:

$$\varepsilon = \frac{e}{d\Delta t}$$

where e is the positional error (assumed independent) and Δt the fix interval. Positively correlated errors – as is likely if the buoys are calculating their positions from the same GPS satellites – can cancel, reducing uncertainty. This suggests that the fix interval could be significantly reduced without errors becoming significant. With SA-era accuracy, a timestep of five minutes would produce an error of 1×10^{-6} s^{-1} and post-SA, i.e. current, accuracy levels would allow this sampling interval to be reduced still further, to less than one minute for the same error. It would be interesting to discover whether the upward trend in the RMS magnitude continues down to this level. If the driving factor in these oscillations is a mechanism such as translation by wave radiation pressure, then we would expect a positive result, given the short period of the waves (7–8 s). Such a short interval would also resolve any oscillatory motion at internal wave periods.

5. Conclusions

[49] The new results show that DKP values in the literature underestimate relative motions near the ice edge by at least an order of magnitude and up to two orders of magnitude for unconsolidated ice. This has major implications for model rheologies of the region. Crushing thin ice during convergent events and exposing sea surface during divergence cycles is a particularly efficient ice growth process at high-frequencies [*Koentopp et al.*, 2005; *Padman and Kottmeier*, 2000] and is often termed the "ice accordion". The new values therefore imply much increased ocean-atmosphere heat flux, ice growth and salt rejection to the ocean in the ice edge region.

[50] The mechanism behind the very high amplitudes observed appears open to question at present, with waves – either internal or surface gravity – appearing the most likely candidates. Further field measurements, using similar buoys transmitting very high frequency GPS positions are required to resolve this question. Additional instrumentation, in the form of a current meter to resolve the ice-water velocity would also be desirable.

[51] **Acknowledgments.** Work was supported by the UK Natural Environment Research Council, under grant GR3/12952. We are grateful to the Alfred Wegener Institut für Polar- und Meeresforschung, Bremerhaven, for the opportunity to work from F/S *Polarstern* during the field experiment and thank the captain and crew for their kind cooperation. We also thank Max Coon (North West Research Associates) for his invaluable help and advice during the field experiment.

References

Crane, D., and P. Wadhams (1996), Sea-ice motion in the Weddell Sea from drifting buoy and AVHRR data, *J. Glaciol.*, *42*(141), 249–254.

Doble, M. J., M. D. Coon, and P. Wadhams (2003), Pancake ice formation in the Weddell Sea, *J. Geophys. Res.*, *108*(C7), 3209, doi:10.1029/2002JC001373.

Geiger, C. A., S. F. Ackley, and W. D. Hibler III (1998), Sea ice drift and deformation processes in the Western Weddell Sea, in *Antarctic Sea Ice: Physical Processes, Interactions and Variability*, edited by M. O. Jeffries, pp. 141–160, AGU, Washington, D. C.

Geiger, C. A., Y. Zhao, A. K. Liu, and S. Hakkinen (2000), Large scale comparison between buoy and SSM/I drift and deformation in the Eurasian Basin during winter 1992–1993, *J. Geophys. Res.*, *105*(C2), 3357–3368.

Gordon, A. L., and B. A. Huber (1990), Southern Ocean winter mixed layer, *J. Geophys. Res.*, *95*(C7), 11,655–11,672.

Guest, P. S., and K. L. Davidson (1991), The aerodynamic roughness of different types of sea ice, *J. Geophys. Res.*, *96*(C3), 4709–4721.

Guest, P. S., K. L. Davidson, J. E. Overland, and P. A. Frederikson (1995a), Atmosphere-ocean interactions in the marginal ice zones of the Nordic seas, in *Arctic Oceanography: Marginal Ice Zones and Continental Shelves*, edited by W. O. Smith and J. M. Grebmeier, pp. 51–96, AGU, Washington, D. C.

Guest, P. S., J. W. Glendening, and K. L. Davidson (1995b), An observational and numerical study of wind stress variations within marginal ice zones, *J. Geophys. Res.*, *100*(C6), 10,887–10,904.

Hoeber, H. (1991), Sea-ice dynamics in the Weddell Sea in winter, *Ann. Glaciol.*, *15*, 9–16.

Hopkins, M. A., and H. H. Shen (2001), Simulation of pancake ice dynamics in a wave field, *Ann. Glaciol.*, *33*, 355–360.

Koentopp, M., O. Eisen, C. Kottmeier, L. Padman, and P. Lemke (2005), Influence of tides on sea ice in the Weddell Sea: Investigations with a high-resolution dynamic-thermodynamic model, *J. Geophys. Res.*, *110*, C02014, doi:10.1029/2004JC002405.

Kottmeier, C., and L. Sellmann (1996), Atmospheric and oceanic forcing of Weddell sea ice motion, *J. Geophys. Res.*, *101*(C9), 20,809–20,824.

Kottmeier, C., J. Olf, W. Frieden, and R. Roth (1992), Wind forcing and ice motion in the Weddell Sea region, *J. Geophys. Res.*, *97*(D18), 20,373–20,383.

Kottmeier, C., et al. (1997), Wind, temperature and ice motion statistics in the Weddell Sea, World Clim. Res. Programme, Geneva.

Lange, M. A., and H. Eicken (1991), Textural characteristics of sea ice and the major mechanisms of ice growth in the Weddell Sea, *Ann. Glaciol.*, *15*, 210–215.

Leonard, G. H., H. Shen, and S. F. Ackley (1998), Dynamic growth of a pancake ice cover, in *Proceedings of 14th International Symposium on Ice: Ice in Surface Waters*, edited by H. T. Shen, pp. 891–896, Balkema, Potsdam, New York.

Lindsay, R. W. (2002), Ice deformation near SHEBA, *J. Geophys. Res.*, *107*(C10), 8042, doi:10.1029/2000JC000445.

Liu, A. K., P. W. Vachon, C. Y. Peng, and A. S. Bhogal (1992), Wave attenuation in the marginal ice zone during LIMEX, *Atmos. Ocean*, *30*(2), 192–206.

Longuet-Higgins, M. S., and R. H. Stewart (1964), Radiation stresses in water waves; a physical discussion, with applications, *Deep Sea Res.*, *11*, 529–562.

Martinson, D. G., and C. Wamser (1990), Ice drift and momentum exchange in winter Antarctic pack ice, *J. Geophys. Res.*, *95*(C2), 1741–1755.

Massom, R. A. (1992), Observing the advection of sea ice in the Weddell Sea using buoy and satellite passive microwave data, *J. Geophys. Res.*, *97*(C10), 15,559–15,572.

McPhee, M. (1987), A time-dependent model for turbulent transfer in a stratified oceanic boundary layer, *J. Geophys. Res.*, *92*(C7), 6977–6986.

McPhee, M. G. (1980), An analysis of pack ice drift in summer, in *Sea Ice Processes and Models*, edited by R. S. Pritchard, pp. 62–75, Univ. of Washington Press, Seattle.

Meldrum, D., M. J. Doble, D. Mercer, O. Peppe, P. Wadhams, and J. Wilkinson (2000a), A study of the winter Antarctic marginal ice zone using an innovative ice drifter, in *Oceanology International*, pp. 73–85, Spearhead Exhibitions Ltd, Brighton, U. K.

Meldrum, D. T., D. J. L. Mercer, and O. C. Peppe (2000b), Orbcomm - An Antarctic evaluation, in *Developments in Buoy Technology, Communications and Data Applications: DBCP Scientific and Technical Workshop*, pp. 61–76, World Meteorol. Org., Geneva.

Muench, R. D., P. H. LeBlond, and L. E. Hachmeister (1983), On some possible interactions between internal waves and sea ice in the marginal ice zone, *J. Geophys. Res.*, *88*(C5), 2819–2826.

Onstott, R. G., P. Gogineni, A. J. Gow, T. C. Grenfell, K. C. Jezek, D. K. Perovich, and C. T. Swift (1998), Electromagnetic and physical properties of sea ice formed in the presence of wave action, *IEEE Trans. Geosci. Remote Sens.*, *36*(5), 1764–1783.

Padman, L., and C. Kottmeier (2000), High-frequency ice motion and divergence in the Weddell Sea, *J. Geophys. Res.*, *105*(C2), 3379–3400.

Pedersen, L. T., and M. D. Coon (2004), A sea ice model for the marginal ice zone with an application to the Greenland Sea, *J. Geophys. Res.*, *109*, C03008, doi:10.1029/2003JC001827.

Ruhmer, R. R., R. Crissman, and A. Wake (1979), Ice transport in the great lakes, Great Lakes Environ. Res. Lab., Ann Arbor, Mich.

Shen, H. H., and S. F. Ackley (1995), A laboratory-produced pancake ice cover in a two-dimensional wave field, *Antarctic J.*, *30*, 106–107.

Thomas, D. (1999), The quality of sea ice velocity estimates, *J. Geophys. Res.*, *104*(C6), 13,627–13,652.

Thorndike, A. S., and R. Colony (1982), Sea ice motion in response to geostrophic winds, *J. Geophys. Res.*, *87*(C8), 5845–5852.

Uotila, J., T. Vihma, and J. Launianen (2000), Response of the Weddell Sea pack ice to wind forcing, *J. Geophys. Res.*, *105*(C1), 1135–1151.

Vihma, T., and J. Launianen (1993), Ice drift in the Weddell Sea in 1990–1991 as tracked by a satellite buoy, *J. Geophys. Res.*, *98*(C8), 14,471–14,485.

Vihma, T., J. Launianen, and J. Uotila (1996), Weddell Sea ice drift: Kinematics and wind forcing, *J. Geophys. Res.*, *101*(C8), 18,279–18,296.

Wadhams, P. (1973), Attenuation of swell by sea ice, *J. Geophys. Res.*, *78*, 3552–3563.

Wadhams, P., and V. A. Squire (1986), The effect of the marginal ice zone on the directional wave spectrum of the ocean, *J. Phys. Oceanogr.*, *16*(2), 358–376.

Wadhams, P., M. A. Lange, and S. F. Ackley (1987), The ice thickness distribution across the Atlantic sector of the Antarctic Ocean in midwinter, *J. Geophys. Res.*, *92*(C13), 14,535–14,552.

Wadhams, P., V. A. Squire, D. J. Goodman, A. M. Cowan, and S. C. Moore (1988), The attenuation rates of ocean waves in the marginal ice zone, *J. Geophys. Res.*, *93*(C6), 6799–6818.

Wamser, C., and D. G. Martinson (1993), Drag coefficients for winter Antarctic pack ice, *J. Geophys. Res.*, *98*(C7), 12,431–12,437.

Wilkinson, J., and P. Wadhams (2003), A salt flux model for salinity change through ice production in the Greenland Sea and its relationship to winter convection, *J. Geophys. Res.*, *108*(C5), 3147, doi:10.1029/2001JC001099.

Worby, A. P., R. A. Massom, I. Allison, V. I. Lytle, and P. Heil (1998), East Antarctic sea ice: A review of its structure, properties and drift, in *Antarctic Sea Ice: Physical Processes, Interactions and Variability*, edited by M. O. Jeffries, pp. 41–67, AGU, Washington, D. C.

M. J. Doble and P. Wadhams, Department of Applied Mathematics and Theoretical Physics, University of Cambridge, Wilberforce Road, Cambridge CB3 0WA, U.K. (m.j.doble@damtp.cam.ac.uk)